

1 Measurement of Muon neutrino Charged-Current
2 Neutral Pion Production at ICARUS

3 Lane Kashur

4 January 26, 2025

5 **Abstract**

6 Begin abstract

7
8 End abstract

9 **Contents**

10	1 Introduction	2
11	1.1 Measurement	2
12	1.2 Data and Monte Carlo Samples	3
13	1.2.1 Data Quality Cuts	3
14	1.2.2 Unblinding Strategy	4
15	2 ν_μ CC π^0 Selection	4
16	2.1 Signal Definition	4
17	2.2 Selection Cuts	4
18	2.3 Selection Performance	5
19	2.4 Variables of Interest	7
20	2.4.1 Energy Reconstruction	7
21	2.4.2 Muon Observables	9
22	2.4.3 Photon Observables	10
23	2.4.4 Neutral Pion Observables	10
24	3 Systematic Uncertainties	11
25	3.1 Flux Uncertainties	11
26	3.2 Cross Section Uncertainties	12
27	3.3 Detector Uncertainties	12
28	4 Data/Monte Carlo Comparisons	12

29	5 Cross Section Measurement	12
30	5.1 Cross Section Extraction Procedure	12
31	5.2 Results	12
32	6 Conclusions	12
33	Appendices	12
34	A Data Quality Cuts	12
35	B Raw Signal Processing and Calibration	12
36	C Machine Learning Reconstruction	12
37	C.1 Point Classification	13
38	C.2 Formation of Particles and Interactions	13
39	C.3 Post-Processors	13

40 1 Introduction

41 Serving as the far detector for the Short-Baseline Neutrino (SBN) Program,
42 ICARUS is poised to address anomalous results from the LSND and MiniBooNE
43 experiments, where excesses of electron-like events could possibly be interpreted
44 as originating from light sterile neutrinos. One key to resolving these anomalies
45 is the search for electron neutrinos in a predominantly muon neutrino beam,
46 for which ICARUS and other detectors in the SBN suite rely on liquid-argon
47 time projection chamber (LArTPC) technology. With excellent calorimetry
48 and fine-grained spatial resolution, LArTPCs enable ICARUS to make precise
49 measurements of electron neutrino interactions as part of a robust neutrino
50 oscillation program.

51 Equally important to the success of ICARUS is characterization of back-
52 grounds that can mimic the electron neutrino appearance signal. Primary
53 among these backgrounds is the production of neutral pions, or π^0 s, which decay
54 electromagnetically to photons. π^0 production is mostly attributed to baryon
55 resonance (RES) in neutrino-nucleon interactions that occur at few-GeV scale,
56 which is also the energy at which the upcoming Deep Underground Neutrino
57 Experiment (DUNE) neutrino beam peaks at. An ICARUS analysis centered
58 around neutral pions therefore not only informs us about the SBN Program's
59 most significant background, but also provides a probe for the types of neutrino
60 interactions expected at next-generation oscillation experiments.

61 1.1 Measurement

62 In this document, we report the flux-averaged differential cross section measure-
63 ment of muon neutrino charged-current interactions with a single π^0 in the final
64 state on argon, hereafter referred to as ν_μ CC π^0 interactions:

$$\nu_\mu + Ar \rightarrow \mu^- + \pi^0 + 0\pi^\pm + X. \quad (1)$$

Here, X represents any final state particles that are not muons or charged pions. The omission of charged pions in the final state aims to exclude charged-current coherent pion production from the analysis, therefore allowing the cross section measurement to probe the resonant production mode that is more relevant to the SBN Program.

Few charged-current π^0 measurements exist on liquid argon, and a high statistics cross section measurement of this channel at ICARUS will help constrain uncertainties in modeling resonant neutrino-nucleon interactions. We present the ν_μ CC π^0 differential cross section measurement as a function of muon and neutral pion kinematic variables, with event selection being carried out by a novel machine-learning reconstruction pipeline. Benefiting from high purity and excellent resolution in reconstructed variables, the extraction of a precise, finely-binned differential cross section is made possible.

1.2 Data and Monte Carlo Samples

This analysis utilizes ICARUS data collected from the Booster Neutrino Beam (BNB) between winter 2022 and spring 2023 (ICARUS Run 2). This collection period corresponds to approximately 2.05×10^{20} protons on target (POT). The analysis can be easily extended to the Neutrinos at the Main Injector (NuMI) beam, and will be in the future as data processing and treatment of systematic uncertainties allows. Data is processed through the ICARUS reconstruction chain (see Appendices A & B) with *icaruscode* software version v09.89.01.01.

Monte Carlo simulation consisting of BNB neutrinos (produced with GENIE) and cosmics (produced with CORSIKA) is used to assess selection performance. This Monte Carlo sample corresponds to 1.74×10^{10} POT. To evaluate the impact from cosmic activity that occurs within the $9.6 \mu s$ BNB beam gate, off-beam data is used (To-do). A summary of production files used in this analysis is shown in Table 1.

Table 1: Data/Simulation Productions used for ν_μ CC π^0 analysis.

	Production	POT
Data (on-beam)	BNB Run 2 On-Beam Majority Trigger	2.05×10^{20}
Data (off-beam)	BNB Run 2 Off-Beam Majority Trigger	N/A
Simulation	BNB ν + Cosmics	1.74×10^{20}

1.2.1 Data Quality Cuts

To ensure the data used in this analysis is of physics quality, a number of data quality cuts are enforced. Namely, any data collection runs that were subject to DAQ issues or happened during detector hardware updates are removed from consideration. Additionally, cuts are made to avoid detector features that are yet to be modeled in simulation, including a field cage short in the EE TPC

98 and a cable hanging in the active volume of the WW TPC. A full description
99 of all data quality cuts used in this analysis can be found in Appendix A.

100 1.2.2 Unblinding Strategy

101 The official blinding policy of the ICARUS collaboration (doc-db 34523) states
102 that 90 percent of data is to remain blinded until any analysis is finalized.
103 To comply with this policy, all analysis toward the ν_μ CC π^0 cross section
104 measurement shown in this document only uses the 10 percent of Run 2 data
105 that has been unblinded. An exception has been made for data collection run
106 9435, which has been completely unblinded for the purpose of visual scanning.

107 Pending approval from the physics coordinators and event selection working
108 group, we request access to...(To-do)

109 2 ν_μ CC π^0 Selection

110 2.1 Signal Definition

111 The ν_μ CC π^0 signal definition encompasses charged-current neutrino interac-
112 tions occurring within the fiducial volume of the detector and containing

- 113 • exactly one primary muon
- 114 • exactly zero charged pions
- 115 • exactly one neutral pion
- 116 • any number of particles that are not muons or pions.

117 This signal definition applies to final state particles, or particles exiting the tar-
118 get nucleus post-final state interactions (FSI). The fiducial volume requirement
119 applies to the neutrino interaction vertex, which must be 25 cm from detector
120 boundaries in the drift and vertical directions, 30 cm from the upstream detector
121 face, and 50 cm from the downstream face.

122 Additional requirements are placed on the signal definition to ensure tracking
123 thresholds are met and selection purity and efficiency are optimized. These are
124 referred to as phase space constraints and include:

- 125 • $p_\mu \geq 226$ MeV/c
- 126 • $p_{\pi^0} \geq 100$ MeV/c.

127 2.2 Selection Cuts

128 When selecting ν_μ CC π^0 interactions, cuts are made on various reconstructed
129 outputs to narrow the list of candidate interactions. Included are cuts on:

- 130 • Fiducial volume: Reconstructed vertex is required to be inside fiducial
131 volume (defined in signal definition).

- 132 • Topology: Interaction contains exactly one primary muon, zero primary
133 charged pions, and two or three primary photons as reported by the
134 machine-learning reconstruction chain's primary particle classification and
135 particle identification algorithms. Particles also meet phase space require-
136 ments of the signal definition. In the case of three photons, the pair of
137 photons with reconstructed invariant mass closest to m_{π^0} is chosen to
138 represent the neutral pion candidate.
- 139 • Neutral pion mass: Invariant diphoton mass < 400 MeV in order to reject
140 η mesons.
- 141 • Flash time: Interaction is associated with an optical flash that is in-time
142 with BNB beam gate, as determined by the OpT0Finder algorithm.

143 2.3 Selection Performance

144 Selection performance is assessed using the BNB ν + Cosmic MC sample and
145 off-beam BNB Run 2 data. The metrics that have been evaluated are efficiency -
146 the fraction of true signal interactions that are matched to selected interactions,
147 and purity - the fraction of selected interactions that are matched to true signal
148 interactions. Figure 1 shows the selection efficiency for ν_μ CC π^0 events before
149 muon and neutral pion momentum thresholds are applied. The sharp drop-offs
150 at 226 MeV/c and 100 MeV/c for the muon and neutral pion distributions,
151 respectively, motivate the phase space constraints of the signal definition.

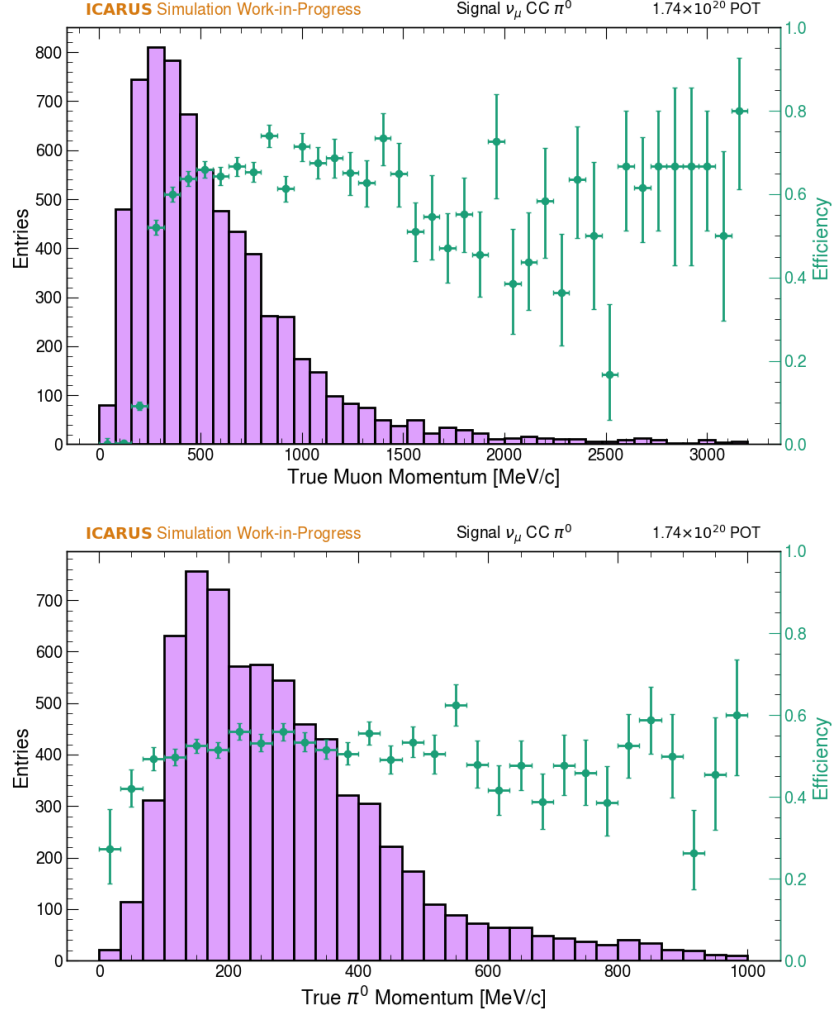


Figure 1: Efficiency of selecting signal events as a function of muon and neutral pion momentum.

After phase space constraints are placed, the selection achieves an efficiency of 59.68% and a purity of 84.33%. Efficiency and purity for each selection cut are shown in Table 2. Inefficiencies and impurities are primarily driven by PID failures, which are further characterized in 2. Background topologies can also be seen in Section 2.4.

Table 2: Purity and efficiency for ν_μ CC π^0 Selection Cuts

Selection Cut	Efficiency [%]	Purity [%]
No Cut	100	0.09
In-Time Flash	96.6	2.64
Fiducial Volume	95.73	4.03
Topology	59.77	83.18
$m_{\gamma\gamma} < 400 \text{ MeV}/c^2$	59.68	84.33

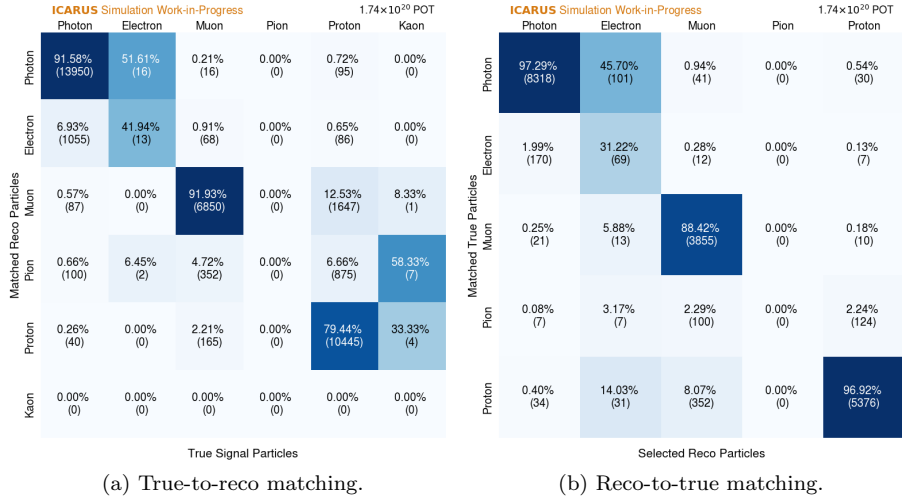


Figure 2: Confusion matrices for particle identification, as determined by the SPINE machine-learning chain.

2.4 Variables of Interest

In this section, the kinematic observables used in the single differential cross section measurement are discussed. Included are the momenta of the final state muon and neutral pion, as well as the angles these particles make with the BNB. An additional variable, the invariant diphoton mass, is examined as it serves as a useful standard candle in the calibration of the electromagnetic shower energy scale. First, however, the methods used to estimate the energy (and momentum) of the reconstructed particles of interest is detailed.

2.4.1 Energy Reconstruction

To estimate the momentum of the reconstructed muon, it is first necessary to reconstruct its energy, for which a “best estimate” approach is taken. For muons contained within the active detector volume, momentum is calculated using the Continuous Slowing Down Approximation (CSDA) that relates a particle’s kinetic

energy to its range in a material. For momentum estimation of exiting muons, the degree of multiple coulomb scattering (MCS) along the track is instead used. Figure 3 shows how each muon momentum estimate compares with true muon momentum in simulation.

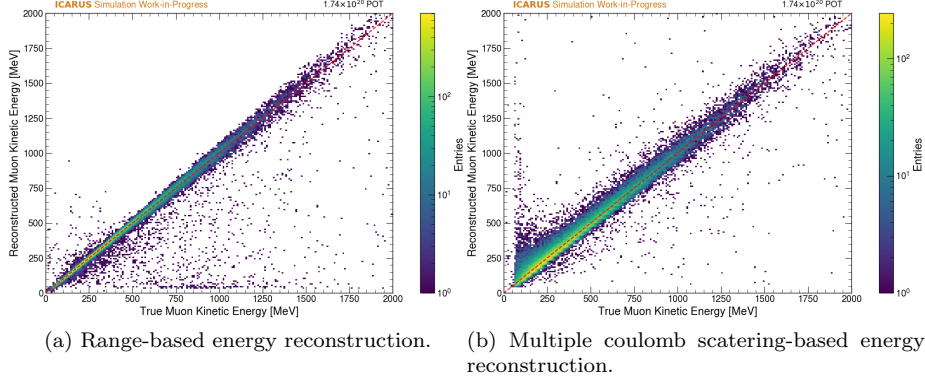


Figure 3: Comparisons of reconstructed and true muon kinetic energy for a selection of contained muons in ICARUS simulation.

Unlike muons, neutral pions do not directly ionize the detector medium. The neutral pion momentum must therefore be inferred from the electromagnetic showers instigated by the photons it decays to. Shower energy (and momentum) is estimated calorimetrically by summing charge depositions belonging to the shower and accounting for various detector effects:

$$E_{shower} = W_i \left[\frac{MeV}{e^-} \right] \cdot C_{cal} \left[\frac{e^-}{ADC} \right] \cdot C_{adj} \cdot \frac{1}{R} \cdot \sum_{dep} e^{\frac{t_{drift}}{\tau}} \cdot dep[ADC], \quad (2)$$

where

- W_i is the work function for argon
- C_{cal} converts charge units from ADC to electrons
- C_{adj} accounts for missing energy due to subthreshold charge and clustering effects in reconstruction
- R is the recombination factor
- τ is the electron lifetime
- dep is charge in units of ADC.

The shower correction factor, C_{adj} , is derived from a study of contained photons in simulation. Figure 4a shows the ratio of reconstructed photon energy (from equation 2) to true photon energy. As this ratio is mostly flat across different energies, a constant correction factor is chosen. Reconstructed photon

191 energy is again compared to true photon energy in 4b, showing agreement after
 192 the correction factor is applied. It is also worth noting that since the analysis
 193 signal definition does not require showers to be contained, an additional correc-
 194 tion factor is needed to correct for missing energy in exiting showers. A study
 195 for deriving this factor is ongoing with results expected soon.

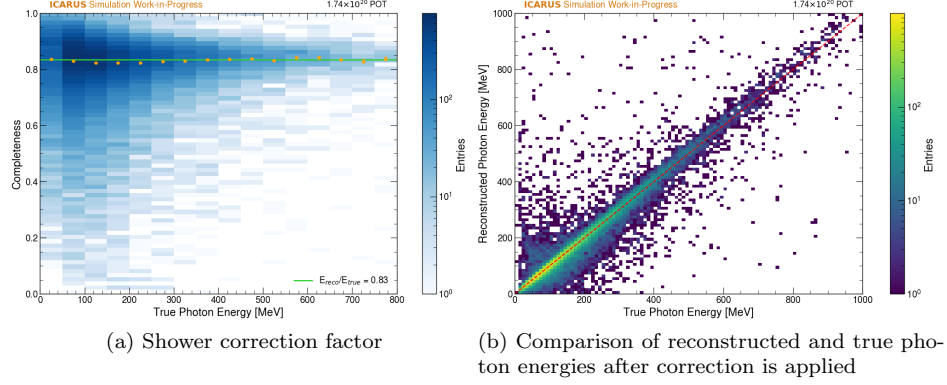


Figure 4: Study of reconstructed electromagnetic shower energy.

196 2.4.2 Muon Observables

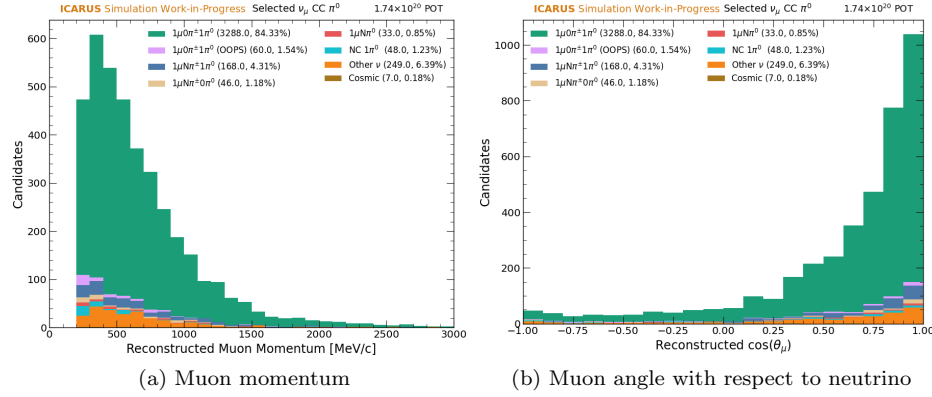


Figure 5: Muon observables chosen for analysis

2.4.3 Photon Observables

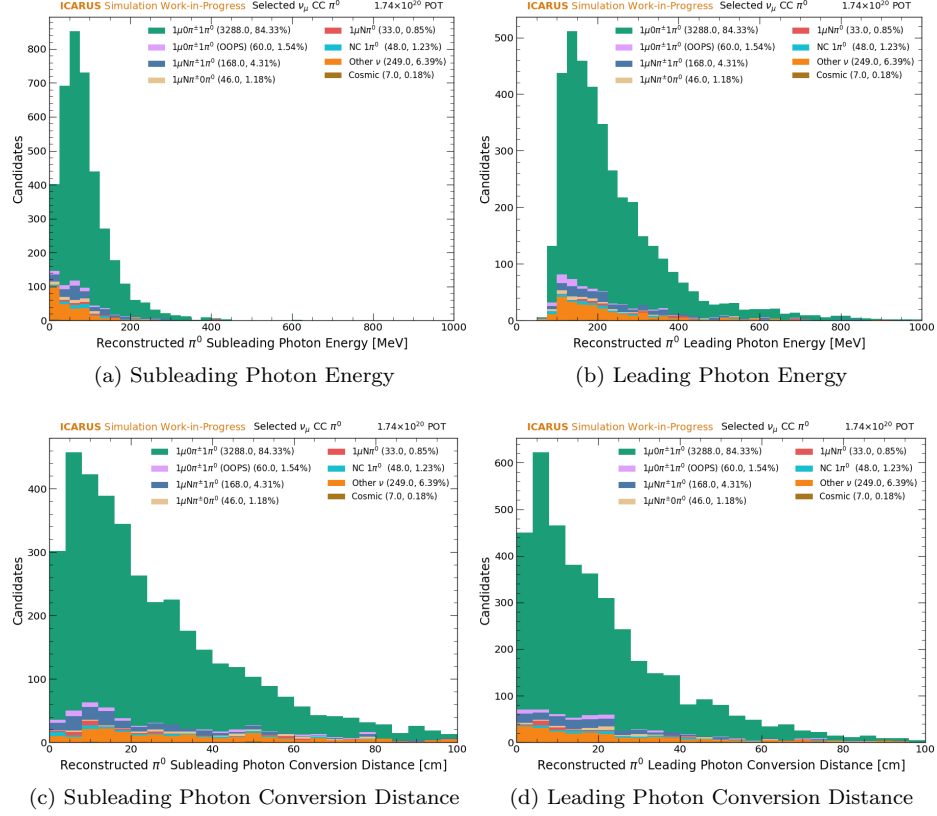


Figure 6: Photon observables chosen for analysis (not directly used in cross section measurement)

2.4.4 Neutral Pion Observables

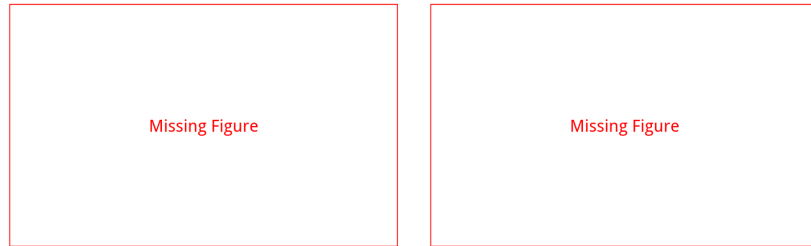


Figure 7: A missing figure.



Missing Figure

Figure 8: A missing figure.

3 Systematic Uncertainties

The systematic uncertainties relevant to this analysis are divided into three categories: (1) beam flux, (2) interaction modeling, and (3) detector response modeling. In this section, the methods for addressing each uncertainty are discussed.

3.1 Flux Uncertainties

The BNB flux at ICARUS is based on predictions from the MiniBooNE collaboration, which used the Geant4 simulation tool kit to model the propagation of particles produced in proton beam-target interactions [1]. Treatment of flux uncertainties, which arise from sources like hadron production, hadronic secondary interactions within the beam target, and beam focusing, are handled with a many-universes technique. In this approach, uncertainties are determined by varying the underlying parameters from each source simultaneously in a set of “universes” to construct a covariance matrix. The full set of parameters and the uncertainties they are varied within are shown in Table 3.

Table 3: Purity and efficiency for ν_μ CC π^0 Selection Cuts

Parameter	Uncertainty	Other
pi production	0%	0
pi production	0%	2.64
K production	0%	4.03
K production	0%	83.18

214 3.2 Cross Section Uncertainties

215 3.3 Detector Uncertainties

216 4 Data/Monte Carlo Comparisons

217 5 Cross Section Measurement

218 5.1 Cross Section Extraction Procedure

219 5.2 Results

220 6 Conclusions

221 References

- 222 [1] A. A. A.-A. et al. (MiniBooNE Collaboration), “Neutrino flux prediction
223 at miniboone”, Phys. Rev. D 79, 072002 (2009).
- 224 [2] F. Drielsma, K. Terao, and L. D. and Dae Heun Koh, “Scalable, end-to-end,
225 deep-learning-based data reconstruction chain for particle imaging detec-
226 tors”, (2021).

227 Appendices

228 A Data Quality Cuts

229 B Raw Signal Processing and Calibration

230 C Machine Learning Reconstruction

231 In this section, neutrino event reconstruction is discussed. For information on
232 raw signal processing and calibration, see Appendix B. Reconstruction of neu-
233 trino events is handled by the end-to-end, machine-learning based reconstruction
234 chain known as SPINE (Scalable Particle Imaging with Neural Embeddings) [2].

As input, SPINE takes an image of 3D charge depositions within the detector, which is then operated on by a series of neural networks to carry out point classification and formation of particle and interaction objects.

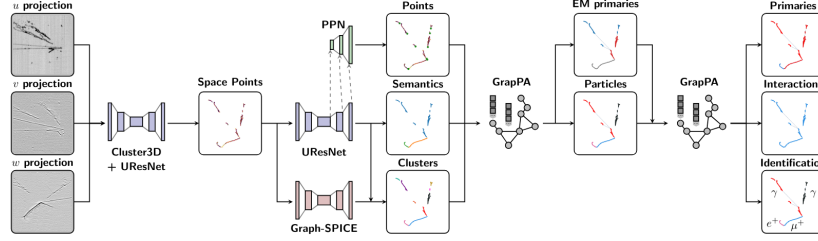


Figure 9: The SPINE reconstruction chain.

C.1 Point Classification

Point classification refers to the classification of 3D space points into abstract particle classes and the identification of points of interest. Convolution neural networks (CNNs) are used for these tasks, beginning with the removal of tomographic reconstruction artifacts by the

C.2 Formation of Particles and Interactions

C.3 Post-Processors